

# Universal and non-universal features in coarse-grained models of flow in disordered solids

Alexandre Nicolas,<sup>a,b</sup> Kirsten Martens,<sup>a,b</sup> Lydéric Bocquet,<sup>c</sup> and Jean-Louis Barrat<sup>a,b,d</sup>

Received Xth XXXXXXXXXXXX 20XX, Accepted Xth XXXXXXXXXXXX 20XX

First published on the web Xth XXXXXXXXXXXX 200X

DOI: 10.1039/b000000x

We study the two-dimensional (2D) shear flow of amorphous solids within variants of an elastoplastic model, paying particular attention to spatial correlations and time fluctuations of, e.g., local stresses. The model is based on the local alternation between an elastic regime and plastic events during which the local stress is redistributed. The importance of a fully tensorial description of the stress and of the inclusion of (coarse-grained) convection in the model is investigated; scalar and tensorial models yield very similar results, while convection enhances fluctuations and breaks the spurious symmetry between the flow and velocity gradient directions, for instance when shear localisation is observed. Besides, correlation lengths measured with diverse protocols are discussed. One class of such correlation lengths simply scale with the spacing between homogeneously distributed, simultaneous plastic events. This leads to a scaling of the correlation length with the shear rate as  $\dot{\gamma}^{-1/2}$  in 2D in the athermal regime, regardless of the details of the model. The radius of the cooperative disk, defined as the near-field region in which plastic events induce a stress redistribution that is not amenable to a mean-field treatment, notably follows this scaling. On the other hand, the cooperative volume measured from the four-point stress susceptibility and its dependence on the system size and the shear rate are model-dependent.

## 1 Introduction

The onset of rigidity in a liquid cooled below its glass transition temperature, as well as in granular matter packed more and more densely, is accompanied by a growing, presumably diverging correlation length<sup>1,2</sup>. To some extent, the situation is similar to the onset of flow in an amorphous solid. Indeed, flow, and the ensuing fluidisation, of the solid drives it away from the critical elastic state that exists at vanishing shear rate<sup>3</sup>. Diverging correlation lengths are then expected<sup>4–6</sup> when the shear rate goes to zero in the absence of thermal fluctuations<sup>7</sup>.

Extensive experimental research has been conducted to unveil the microscopic details of the slow shear flow of these amorphous materials, from the early works of Argon<sup>8</sup> and Princen<sup>9</sup> on bubble rafts and foams, to the more recent confocal microscopy observations of colloids by Schall and co-workers<sup>10</sup> and the diffusive wave spectroscopy imaging of granular matter<sup>11</sup>. Numerical studies have also been largely contributed to our present understanding<sup>12,13</sup>.

It is now clear that the analogy with the glass (or jamming) transition remains qualitative. In particular, while complex

collective motion on a large scale is observed around the jamming point, the onset of flow in an amorphous solid is characterised by local rearrangements of a handful of particles that induce a long-range elastic deformation in the material, which may trigger new rearrangements in an avalanche-like process (see Baret et al.<sup>14</sup> and references therein).

The enticing simplicity of this scenario has led to the emergence of multiple models. A first class of models explicitly discard spatial correlations and resort to a mean-field-like approach in which the flow is described in terms of hops between “traps” (metastable configurations) that are facilitated by shear. The free volume theories of Spaepen and others, the Shear Transformation Zone theory<sup>15,16</sup>, the Soft Glassy Rheology model<sup>17</sup>, Hébraud and Lequeux’s equations<sup>18</sup> all fall into this category, in spite of the differences in the way they model the “traps”, or the flow defects, and assess the hopping rates. In recognition of the importance of flow heterogeneities, efforts have been made to extend these theories beyond the homogenous, mean-field approximation. This is generally achieved through the inclusion of a diffusive term in the equations<sup>5,19,20</sup>. The diffusion-extended equations have proved helpful in describing the striking manifestations of spatial cooperativity in experiments<sup>20–22</sup>.

Still, one may nurture doubts about the adequacy of a simple diffusive term in situations where heterogeneities interact via long-range (elastic) interactions and fluctuations are large<sup>23</sup>. This issue is addressed by another line of modelling,

<sup>a</sup> Univ. Grenoble Alpes, LIPhy, F-38000 Grenoble, France

<sup>b</sup> CNRS, LIPhy, F-38000 Grenoble, France

<sup>c</sup> ILM, Université de Lyon; UMR 5586 Université Lyon 1 et CNRS, F-69622 Villeurbanne, France

<sup>d</sup> Institut Laue-Langevin, 6 rue Jules Horowitz, BP 156, F-38042 Grenoble, France

namely lattice-based elastoplastic models<sup>14,24,25</sup>, pioneered by Chen & Bak<sup>3</sup>, initially for the description of earthquakes, and Argon & Bulatov<sup>26–28</sup>. (Also see works by Homer & Schuh<sup>29,30</sup> for a similar, but off-lattice, approach). However, it has been remarked<sup>31</sup> that the relevance of such models remains unclear owing to the vast technical simplifications that they involve: generally, they are two-dimensional (2D), they reduce the tensorial stress to a scalar quantity and neglect the displacements of the elastoplastic blocks as the material is deformed.

In this contribution, we propose a detailed analysis of the importance of the latter two aspects, namely the tensoriality of the stress and convection, in an elastoplastic model. In particular, we shall quantitatively probe the spatial correlations in the flow and the temporal fluctuations, (both of which are omitted in purely mean-field approaches).

In Section 2, we clarify the general, continuum mechanics-based framework of our model. We also show how convection can be implemented in 2D mesoscopic models, and derive the relevant formulae for the propagators. In order to best evidence the importance of the tensorial nature of stress and the role of convection, we present a simple (but phenomenologically rich) model in Section 3. The following section is dedicated to the computation of diverse correlation lengths. Finally, in Section 5, the probabilities involved in the model are refined so as to make it more realistic in terms of the microscopic processes that have been evidenced, and we assess how general the scalings we have derived for the correlation lengths are.

## 2 Description of the model

### 2.1 General framework

The picture that emerged from the early experimental works on bubble rafts of Argon<sup>8</sup> and Princen<sup>32</sup>, and that has since received ample confirmation from the observation of diverse amorphous solids under slow shear<sup>10,11</sup> as well as numerical simulation of these systems<sup>33,34</sup>, revolves around localised rearrangements of particles bursting in a mostly elastic medium, provided that the material is clearly solid at rest, i.e., far enough from the glass transition or the jamming point. On account of the shear geometry, these plastic events are essentially tantamount to a relaxation of the local shear stress (via particle rearrangement), although a transient, or even durable, local dilation may occur simultaneously.

Let us first recall how this scenario can be interpreted in the framework of continuum mechanics. More details can be found in previous publications<sup>35,36</sup>.

The elastic medium is characterised by incompressibility and linear elasticity\*, viz.

$$\begin{cases} \nabla \cdot u = 0 \\ \nabla \cdot \sigma^{(0)} - \nabla p^{(0)} = 0 \end{cases} \quad (1)$$

where  $u$  is the displacement field,  $\sigma$  is the elastic stress tensor, and  $p$  is the pressure. If one introduces the linear strain tensor  $\varepsilon = \frac{\nabla u + \nabla u^T}{2}$ , incompressibility dictates that  $\varepsilon_{yy} = -\varepsilon_{xx}$ ; this allows us to use the following condensed notation, under the assumption of isotropy of the medium:  $\sigma^{(0)} = 2\mu \begin{pmatrix} \varepsilon_{xx} \\ \varepsilon_{xy} \end{pmatrix}$ , where  $\mu$  is the shear modulus.

When a plastic event occurs in a region  $S$ , the system loses track of the reference elastic configuration in this region, so that the material is locally fluidised. Region  $S$  is then dominated by dissipative forces  $\sigma_{\text{diss}}$ , which counter the relaxation of the stress  $2\mu\varepsilon_{\partial S}$  locally applied by the surrounding medium. For simplicity, we assume that dissipation is linear in the shear rate,  $\sigma_{\text{diss}} = 2\eta_{\text{eff}}\dot{\varepsilon}^{(\text{pl})}$ , with  $\eta_{\text{eff}}$  an effective viscosity, and we neglect the (subdominant) elastic forces within  $S$  for all the duration of the plastic event. Then, force balance at the boundary  $\partial S$  reads, in the absence of inertia,

$$2\mu\varepsilon_{\partial S} = 2\eta_{\text{eff}}\dot{\varepsilon}^{(\text{pl})}. \quad (2)$$

The plastic strain  $\dot{\varepsilon}^{(\text{pl})}$  (per unit time) deforms the boundary  $\partial S$ , thereby inducing an additional elastic deformation  $\dot{\varepsilon}^{(1)}$  in the medium. To leading order, the increments of deformation  $\dot{\varepsilon}^{(1)}(r)$  and pressure  $\dot{p}^{(1)}(r)$  in the matrix per unit time can be estimated by replacing the *plastic* inclusion with an *elastic* inclusion bearing an eigenstrain<sup>†</sup> (per unit time) equal to the plastic strain (per unit time)  $\dot{\varepsilon}^{(\text{pl})}$ . It immediately follows that,

$$2\mu\nabla \cdot (\dot{\varepsilon}^{(1)} - \dot{\varepsilon}^{(\text{pl})}) - \nabla \dot{p}^{(1)} = 0 \quad (3)$$

Moving back to region  $S$ , since the plastic strain is a *reaction* to the elastic stress  $2\mu\varepsilon_{\partial S}$ , it is expected to lower the elastic strain at the boundary  $\partial S$ . On account of the linearity of the problem, for a small inclusion  $S$ , one can then write

$$\dot{\varepsilon}_{\partial S} = \dot{\varepsilon}_{\partial S}^{(1)} = -g_0\dot{\varepsilon}^{(\text{pl})}, \quad (4)$$

where  $g_0$  is a positive scalar of order 1, whose precise value (in our implementation) will be discussed in Section 3.1. The dynamics of the plastic event are obtained by combining Eqs. 2 and 4,

$$\dot{\varepsilon}_{\partial S} = \frac{-g_0}{\tau}\varepsilon_{\partial S}, \quad (5)$$

where the timescale  $\tau \equiv \eta_{\text{eff}}/\mu$  has been introduced.

---

linear elasticity observed<sup>37</sup>.

† An eigenstrain  $\varepsilon^*$  is defined by the following local elastic relation between stress and strain,  $\sigma = 2\mu(\varepsilon - \varepsilon^*)$ .

\* Only very close to the onset of a plastic event is a significant departure from

## 2.2 Derivation of the elastic propagator

### 2.2.1 In an orthonormal frame

We follow, and extend, the method proposed by Picard et al.<sup>38</sup> to find the Green's function for Eq. 3, i.e., the elastic propagator  $\mathcal{G}^\infty$ .

With the shorthand  $f$  for  $-2\mu\nabla \cdot \dot{\varepsilon}^{(\text{pl})}$ , Eq. 3 can be recast as

$$2\mu\nabla^2 \dot{u}^{(1)} - \nabla \dot{p}^{(1)} + f = 0,$$

For convenience, we drop the (1)-superscripts denoting the increments due to the plastic strain rate  $\dot{\varepsilon}^{(\text{pl})}$ , as well as the dots indicating time derivatives for the rest of this section:

$$2\mu\nabla^2 u - \nabla p + f = 0. \quad (6)$$

The combination of Eq. 6 with the incompressibility condition,  $\nabla \cdot u = 0$ , defines a well-known problem in hydrodynamics, for a (set of) pointwise source term(s)  $f$ . Its solution is most conveniently expressed in Fourier coordinates  $q \equiv (q_x, q_y)$  with the help of the Oseen-Burgers tensor<sup>39</sup>  $\mathcal{O}_j^i(q) = \frac{1}{\mu q^2} \left( \delta_j^i - \frac{q^i q_j}{q^2} \right)$ , where  $i$  and  $j$  denote spatial directions, and we have written, with Einstein's summation convention,  $^\dagger q^2 \equiv q_i q^i$ ,  $i \in \{x, y\}$ , viz.,

$$u^i(q) = \mathcal{O}_j^i(q) f^j(q) = \frac{1}{2\mu q^2} \left( \delta_j^i - \frac{q^i q_j}{q^2} \right) f^j(q) \quad (7)$$

Finally, using  $\sigma_j^i(q) = 2\mu \left[ i \frac{q_j u^i + q^i u_j}{2} - \varepsilon_j^{(\text{pl})i}(q) \right]$ , we arrive at

$$\begin{pmatrix} \sigma_{xx} \\ \sigma_{xy} \end{pmatrix} (q) = 2\mu \mathcal{G}^\infty(q) \cdot \begin{pmatrix} \varepsilon_{xx}^{(\text{pl})} \\ \varepsilon_{xy}^{(\text{pl})} \end{pmatrix} (q)$$

where

$$\mathcal{G}^\infty(q) \equiv \frac{1}{q^4} \begin{bmatrix} -(q_x^2 - q_y^2)^2 & -2q_x q_y (q_x^2 - q_y^2) \\ -2q_x q_y (q_x^2 - q_y^2) & -4q_x^2 q_y^2 \end{bmatrix}. \quad (8)$$

Bear in mind that, under the assumption of incompressibility,  $\varepsilon_{xx} = -\varepsilon_{yy}$ . In real space, the components of the elastic propagator  $\mathcal{G}^\infty$  display a four-fold angular symmetry and an  $r^{-d}$  spatial decay, with  $d$  the dimension of space, in accordance with experimental and numerical evidence<sup>10,40</sup>. (See, e.g., Fig. 1(right) in Ref. <sup>41</sup> for a depiction of  $\mathcal{G}_{22}^\infty$  in real space.)

It is worth noting that, in discretised space, with square mesh size set to unity, only wavenumbers in the first Brillouin zone, viz.,  $q_x, q_y \in ]-\pi, \pi]$ , will be relevant. In addition, periodicity will further restrict the nonzero Fourier modes to multiples of  $\pi/L$ , where  $L$  is the periodic length in the direction under consideration.

### 2.2.2 In a non-orthogonal frame

As convection is to be included in the model, the initially orthonormal frame  $(x, y)$  will be deformed into a non-orthogonal frame  $(x', y') = (x - \gamma y, y)$ , where  $\gamma$  is the average shear strain experienced by the cell, so that the periodic replicas are advected with respect to each another by the flow. In Fourier space, the correspondence between the wavenumbers in the initial and deformed frames reads  $(q'_x, q'_y) = (q_x, q_y + \gamma q_x)$ . Note that in the deformed frame covariant (e.g.,  $q'_x$ ) and contravariant (e.g.,  $q'^x$ ) vector components need not be equal. In Appendix A, the derivation of the elastic propagator  $\mathcal{G}^\infty$  is extended to such a non-orthogonal basis, with the help of the metric tensor in the deformed frame. One arrives at an expression very similar to that derived previously, Eq. 8, where the wavenumbers  $q_x$  and  $q_y$  in the orthonormal frame are simply replaced by their expressions as functions of  $q'_x$  and  $q'_y$ , viz.,

$$\mathcal{G}^\infty(q') \equiv \frac{1}{q'^4} \begin{bmatrix} -(q_x'^2 - q_y'^2)^2 & -2q'_x q_y' (q_x'^2 - q_y'^2) \\ -2q'_x q_y' (q_x'^2 - q_y'^2) & -4q_x'^2 q_y'^2 \end{bmatrix}.$$

The shorthands  $q_y^{(\gamma)} \equiv q'_y - \gamma q'_x$  and  $q'^4 \equiv (q_x'^2 + q_y^{(\gamma)2})^2$  have been employed here.

This last formula brings to completion our effort to derive the propagator for the stress redistribution in a uniform elastic matrix. We now have to posit the rules for the local alternation of elastic regime and plastic events, in light of the phenomenology evidenced experimentally and numerically in the literature.

## 3 Simplistic model

### 3.1 Presentation of the model

Having dealt with the effect of a plastic event, we will now consider the application of a finite strain rate to the material, with a velocity gradient along the  $y$ -direction, so that the time evolution of the local stress is a combination of the response to the applied strain and the stress redistribution due to plastic events,

$$\partial_t \sigma(r, t) = \mu \begin{pmatrix} 0 \\ \dot{\gamma} \end{pmatrix} + \int \mathcal{G}^\infty(r - r') \dot{\varepsilon}^{(\text{pl})}(r', t) dr', \quad (9)$$

where  $\dot{\gamma}$  is the applied shear rate, and  $\dot{\varepsilon}^{(\text{pl})}(r', t) = \frac{\sigma(r', t)}{2\mu\tau}$  if a plastic event is occurring locally (see Eq. 5), 0 otherwise. Note that Eq. 9 also applies to regions undergoing a plastic event, even though  $\sigma$  is then of dissipative nature; the local part of Eq. 9 then simply describes a Maxwell fluid of characteristic time  $\tau/g_0$ , where the value of the (positive)  $g_0$  coefficient introduced in Eq. 4 is given by the (opposites of the) eigenvalues of the local component  $\mathcal{G}^\infty(r - r' = 0)$  in Eq. 9. In our implementation of Eq. 8, these eigenvalues are close to -0.5.

<sup>†</sup> To simplify notations, we shall drop the hats for functions in Fourier space, that is, we shall write  $u(q)$  instead of  $\hat{u}(q) \equiv \iint dx dy u(x, y) e^{-i(q_x x + q_y y)}$ .

Turning to the criteria governing the onset and end of plastic events, we first consider the very simple rules introduced by Picard *et al.*<sup>24</sup> in a scalar version of the model and their straightforward extension to the tensorial case (with  $\epsilon_{xx} \neq 0$ ). Once the maximal shear stress  $\|\sigma\| \equiv \sqrt{\sigma_{xx}^2 + \sigma_{xy}^2}$  in a small region exceeds a given value  $\sigma_y$ , this region has a finite probability to yield. The associated yield rate is set to a constant,  $\tau_{liq}^{-1}$ . We take  $\tau_{liq}^{-1} = \tau^{-1}$ , where  $\tau$  is the characteristic time defined above. Besides, particle rearrangements last for a constant (stress-independent) time  $\tau_{res}$  on average. We choose units of time and stress such that  $\tau = 1$  and  $\mu = 1$ .

Picard and co-workers showed that, in spite of its simplicity, the model displays increasing complexity and cooperativity as the shear rate  $\dot{\gamma}$  tends to zero, while a mean-field-like behaviour is recovered at large applied shear rates<sup>24</sup>. In the following, we measure diverse correlation lengths aimed at quantifying this cooperative behaviour as  $\dot{\gamma}$  decreases, and we assess to what extent our results are altered by the insertion of a tensorial stress or/and convection.

### 3.2 Numerical implementation

Before we proceed, a few words ought to be said about the numerical implementation of the model. The system is discretised into a regular square lattice of  $N = L \times L$  elastoplastic blocks of unit size. At each time step, the stress increments given by Eq. 9 are computed in Fourier space, and then mapped back into real space. For accuracy, we resolve the stresses on a finer mesh, in which each elastoplastic block is made of four subcells. Also note that the computation of the elastic propagator in discrete space may slightly violate the equality of the streamline-averaged shear stresses imposed by static mechanical equilibrium. To recover strict mechanical equilibrium, we add a small *ad hoc* offset to each streamline at every time step. We checked that this procedure has only little impact on both the flow curve and the correlation functions. After receiving their stress increments, blocks may undergo a change of state, with the probabilities given above.

To account for convection, i.e., the advection of blocks along the streamlines, the average shear deformation of the simulation cell is updated at every timestep, *viz.*,  $\gamma_{total} = \dot{\gamma}t + (u_x^{top} - u_x^{bottom})/(y^{top} - y^{bottom})$ , where the non-affine displacements  $u_x^{top}$  and  $u_x^{bottom}$  of the “top” and “bottom” streamlines, with  $x$  the flow direction, have been considered; note that these non-affine displacements average to zero in an infinite system. Because the simulation cell is replicated periodically along both directions, one can always find an appropriate  $\gamma_{total}$  in the range  $]-1/2, 1/2]$ . This defines the deformed frame. Since the flow is not strictly homogeneous, or, equivalently, the deformation is not strictly affine, we must additionally compute the displacement of each streamline so as to be able to shift it adequately with respect to its neighbours. Details pertaining

to the calculation and implementation of this displacement are provided in Appendix B.

### 3.3 Flow curve and spatial organisation as a function of the restructuring time

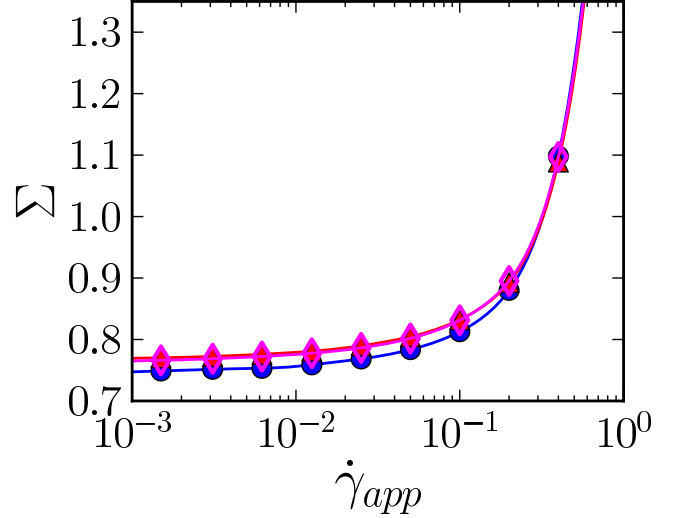


**Figure 1** Flow curves showing the macroscopic shear stress  $\Sigma$  as a function of the applied shear rate  $\dot{\gamma}_{app}$ , for  $\tau_{res} = 1$ . (Open diamonds) static scalar model; (triangles) static tensorial model; (dots) convected tensorial model.

The study of the static (i.e., non-convected) scalar (i.e.,  $\sigma = \begin{pmatrix} 0 \\ \sigma_{xy} \end{pmatrix}$ ) version of the model, as presented in Ref.<sup>41</sup>, showed that at low enough shear rates, a transition from a (macroscopically) homogeneous flow to permanent shear localisation occurs as the restructuring time  $\tau_{res}$  is increased, i.e., when it takes longer to the material to “heal” after a plastic event. Concomitantly with the transition, a stress plateau develops in the flow curve. To what extent is this scenario preserved when a tensorial stress is introduced and convection implemented?

First, we observe on Fig.1 that the flow curve  $\sigma(\dot{\gamma})$  is hardly affected by the extension from a scalar to a tensorial stress; convection does not alter it much either.

The extent of shear-localisation shall be quantified with the following observable:  $\kappa(\Delta\gamma) \equiv (n_{max} - n_{min})/(n_{max} + n_{min})$ , where  $n_{max}$  and  $n_{min}$  denote the maximum and minimum of the line-averaged cumulated plastic activities over strain windows  $\Delta\gamma$ , i.e., the total time spent in the plastic state. To smooth out fluctuations, line averages are further averaged with the first neighbouring lines. With this definition, a vanishing value of  $\kappa$  signals homogeneous flow, whereas  $\kappa = 1$  indicates full shear localisation. Note that even full shear lo-



calisation does not preclude long-term diffusion of the bands, because they are not pinned by a heterogeneity in the driving, as they would be in an experimental Taylor-Couette geometry owing to the larger stress at the rotor. This consideration highlights the necessity to keep  $\Delta\gamma$  finite. On the other hand, for small  $\Delta\gamma$ , spatial correlations are always apparent, even in the absence of macroscopic shear localisation; indeed, plastic events tend to align along “slip lines”, as shown in Fig.2, and consistently with the molecular dynamics simulations reported in Ref.<sup>42</sup>. Therefore, we choose a strain window of width  $\Delta\gamma \approx 10 - 30$ , after the (globally) stationary state has been reached. The qualitative picture is robust to changes in  $\Delta\gamma$ .

The values of the shear-banding observable  $\kappa$  for various restructuring times and applied shear rates are presented in Fig.3. Clearly, the flow is more prone to shear-banding at low applied shear rates and long restructuring times. This is perfectly consistent with our earlier findings in Ref.<sup>41</sup> as well as with the scenario described in Ref.<sup>43</sup>, whereby a long restructuring time (plastic event) leads to a long-time decrease of the local stress, which results in drastic shear-thinning on the macroscopic scale. The apparent decrease of  $\kappa$  at very low shear rates is most probably due to the diffusive motion of the shear band, since the plastic activity is averaged over a fixed strain window, i.e., increasingly large time windows as  $\dot{\gamma}$  decreases.

A comparison between the different versions of the model for a strain window  $\Delta\gamma = 30$  reveals that the inclusion of a tensorial stress in the static model has virtually no effect on the shear-banding diagram (Figure 3a). On the other hand, convection curtails shear-localisation to some extent (Figure 3b), possibly because of the enhancement of stress fluctuations outside the potential shear band, which results in an increased mobility of the latter. The static *vs.* convected discrepancy vanishes when the strain window is reduced, for instance, to  $\Delta\gamma = 5$  (*data not shown*). For smaller system sizes ( $N = 64 \times 64$ ), shear-banding profiles tend to be more diffuse, and shear bands are more mobile, owing to larger fluctuations, but the qualitative picture remains identical.

A major feature of the spatial organisation of the flow is left unnoticed when considering only  $\kappa$ . Without convection, the streamwise and crosswise directions are equivalent, because of the symmetry of the stress tensor. Therefore shear bands are found equivalently in either direction, which conflicts with experimental observations. As expected, enforcing convection breaks the symmetry and only allows shear bands in the flow direction.

The growth of cooperativity with increasing restructuring times  $\tau_{res}$  is also reflected by the distribution of principal directions of plastic events. Let  $\theta \in [-90^\circ, 90^\circ]$  be the corresponding angle with respect to the macroscopic shear (xy) direction, that is,  $\cos(2\theta) = \frac{\sigma_{xy}}{\sigma}$ ,  $\sin(2\theta) = \frac{-\sigma_{xx}}{\sigma}$ , where  $\sigma \equiv$

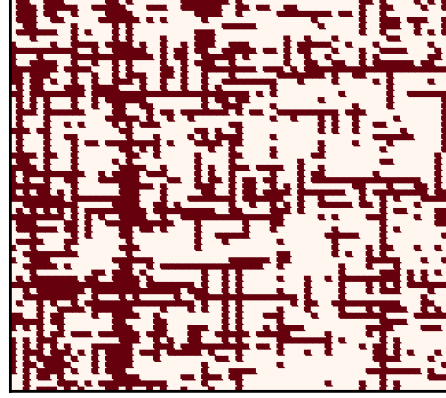


**Figure 2** Map of the plastic activity over a strain window  $\Delta\gamma = 0.4$  in a system without macroscopic shear localisation ( $\tau_{res} = 1$ ,  $\dot{\gamma} = 6.1 \cdot 10^{-3}$ , static tensorial model). Blocks that have yielded at least once over the given strain window are shown in dark. The system is composed of  $64 \times 64$  blocks.

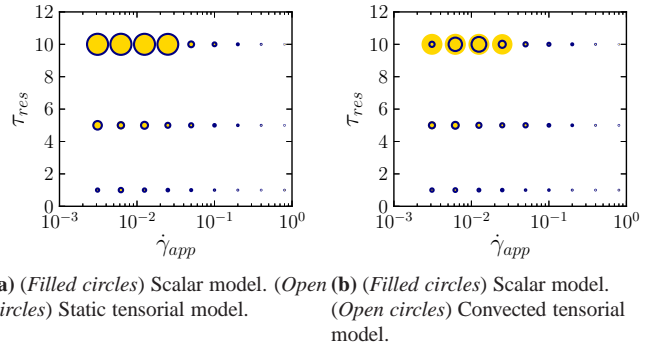


**Figure 3** Dependence of  $\kappa$  on the applied shear rate  $\dot{\gamma}_{app}$  and the restructuring time  $\tau_{res}$ .  $\Delta\gamma = 30$ . Circles are all the larger as the shear-banding observable  $\kappa$  is (proportionally) large. The system consists of  $128 \times 128$  blocks.

$\sqrt{\sigma_{xx} + \sigma_{yy}}$ . In the absence of cooperativity, one expects plastic events to be aligned with the applied shear, hence  $\theta = 0$ . Cooperativity broadens the distribution  $\mathcal{P}(\theta)$ . Indeed, as  $\tau_{res}$  increases from 1 to 10 time units, the standard deviation of the distribution approximately doubles, at a given shear rate. It is also worth noting that switching on convection also results in the doubling of the standard deviation of the distribution, as shown in Fig. 4. Once again, we ascribe this to the enhancement of fluctuations due to convection.

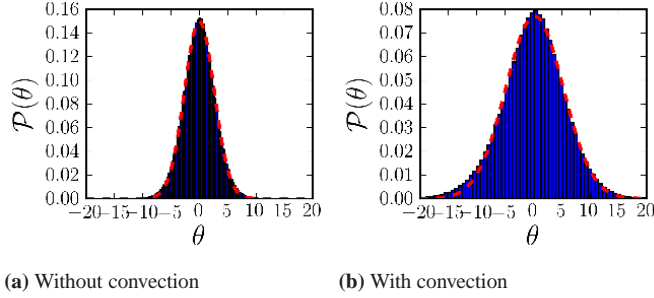


**Figure 4** Distribution of yielding angles  $\theta$  in degrees for  $\tau_{res} = 1$  for tensorial models with and without convection

In the following section, we come back to the original case  $\tau_{res} = 1$ .

## 4 Correlation lengths

### 4.1 Four-point susceptibility $\chi_4$

In glassy systems, instantaneous one-point observables hardly differ from their counterparts in the fluid state, and the search for an observable whose static correlations would distinguish the two states has not borne much fruit so far. On the other hand, time correlations of local observables have proven of great use as order parameters<sup>44</sup>. Here, we study the stress autocorrelation function  $c(r, \Delta t) \equiv \delta\sigma(r, 0) \delta\sigma(r, \Delta t)$ , where  $\delta\sigma \equiv \sigma - \bar{\sigma}$ . Spatial correlations are probed with the four-point correlator

$$\mathcal{G}_4(\Delta r, \Delta t) \equiv \langle c(O, \Delta t) c(\Delta r, \Delta t) \rangle - \langle c(O, \Delta t) \rangle^2, \quad (10)$$

where the brackets denote an average over time, or, equivalently, configurations (since the system is stationary). Note that the above definition is independent of the choice of origin  $O$ .

The precise definition of  $c(r, \Delta t)$  deserves a comment in presence of convection, in which case blocks may move over  $\Delta t$ . In line with the definition of  $c$  as the stress autocorrelator, we adopt a Lagrangian description and compute  $c$  as  $\langle \delta\sigma(r, 0) \delta\sigma(r', \Delta t) \rangle$ , where  $r'$  is the convected position at  $\Delta t$  of the block that was initially at position  $r$ . Note that the same

idea prevailed in Furukawa et al.'s definition<sup>45</sup> of the four-point susceptibility of a system under shear.

Figure 5 shows the spatial profile of  $\mathcal{G}_4$  at  $\dot{\gamma}_{app} = 10^{-3}$  for a delay time  $\Delta t = 0.37$  of the order of the stress autocorrelation time. The profiles for the static versions of the model are indistinguishable with the naked eye, and remain identical if one substitutes  $\sqrt{\sigma_{xx} + \sigma_{yy}}$  for  $\sigma_{xy}$  in the definition of the time correlator  $c$ . They display long branches in the velocity and velocity gradient directions, in accordance with the directions of the positive lobes of the  $xy$ -component of the elastic propagator  $\mathcal{G}^\infty$ . The large spatial extent of these branches is in part due to the periodicity of the system in the two directions.

Adding convection radically changes the picture. Most notably, the symmetry between the  $(Ox)$  (i.e., flow) and  $(Oy)$  (i.e., velocity gradient) directions is broken. The streamline going through the origin keeps a forward-backward ( $x \rightarrow -x$ ) symmetry, but outside this line no such symmetry is preserved. In particular, the branche approximately along  $(Oy)$  direction is tilted, so that a block initially located at position  $-x$  in this branch will be convected to position  $x$  after the lag strain  $\Delta\gamma$ , meanwhile passing through the  $(Oy)$ -lobe of the stress propagator. The distinction between the generic features of  $\mathcal{G}_4$  and those specific to the present model shall be addressed in Section 5.4.

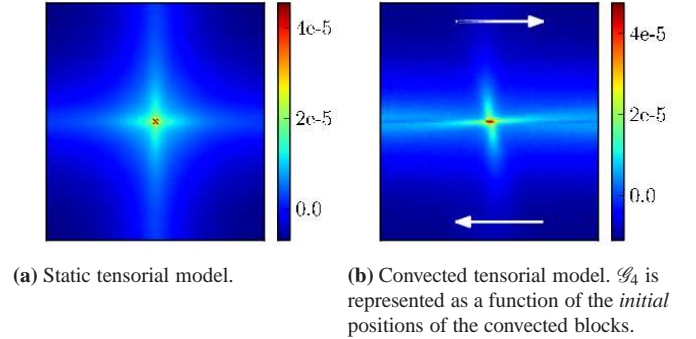


**Figure 5** Spatial profile of the four-point correlator  $\mathcal{G}_4$  at  $\Delta\gamma = 0.37 \approx \Delta\gamma^*$ ,  $\dot{\gamma}_{app} = 10^{-3}$ . System size:  $128 \times 128$ . Because of the comparatively very large value of the stress autocorrelator  $\mathcal{G}_4(0, \Delta t)$ , the central cell has been artificially coloured.

The integral of  $\mathcal{G}_4$  over space, at fixed  $\Delta t$ , yields the four-point susceptibility  $\chi_4$ , that is, the variance of the two-time correlation function with time,  $\chi_4(\Delta t) = V \cdot \text{Var}(C(\Delta t))$ , where  $V$  is the volume of the system,  $C(\Delta t) \equiv V^{-1} \int c(r, \Delta t) dr$ , and the variance operator  $\text{Var}$  has its usual definition,  $\text{Var}(\cdot) \equiv \langle \cdot^2 \rangle - \langle \cdot \rangle^2$ . If the integral is normalised by the value at the origin<sup>44</sup>, viz.,  $\tilde{\chi}_4(\Delta t) \equiv \chi_4(\Delta t) / \mathcal{G}_4(0, \Delta t)$ , it then gives an estimate of the spatial volume in which the stress evolves in a correlated fashion with that at the origin. To illustrate this schematically, suppose that the system consists of

$V/V_{coop}$  entirely correlated, but mutually decorrelated, regions of volume  $V_{coop}$  each. A simple application of the central limit theorem yields

$$\begin{aligned}\tilde{\chi}_4(\Delta t) &= \frac{V \cdot \text{Var}(C(\Delta t))}{\mathcal{G}_4(0, \Delta t)} \\ &\approx V_{coop} \frac{\text{Var}(c(O, \Delta t))}{\mathcal{G}_4(O, \Delta t)} \\ &\approx V_{coop}.\end{aligned}\quad (11)$$

It follows that the peak  $\tilde{\chi}_4^*$  of  $\tilde{\chi}_4(\Delta t)$ , which is reached at a lag time  $\Delta t^*$  close to the stress autocorrelation time, is a measure of the maximal cooperativity in the flow. Here,  $\Delta t^*$  is such that  $\dot{\gamma}\Delta t^* \approx 0.3 - 0.5$  is of the order of the yield strain. The value of  $\mathcal{G}_4(O, \Delta t^*)$  depends even less on the shear rate.

Now, we turn to a more detailed analysis of the variations of the cooperative volume  $\tilde{\chi}_4^*$  with the applied shear rate  $\dot{\gamma}$ , starting with the static models. At rather high shear rates,  $\tilde{\chi}_4^*$  is independent of the system size and exhibits the following shear rate dependence:

$$\tilde{\chi}_4^* \sim \dot{\gamma}^{-\beta}, \quad (12)$$

with  $\beta \approx 0.9$  for both the scalar and the tensorial models. When the shear rate is decreased, the cooperative volume increases, and finally saturates at a value proportional to  $L^{3/2}$  when the whole simulation cell becomes correlated. The transition takes place around a shear rate  $\dot{\gamma}_c$  such that  $\dot{\gamma}_c^{-\beta} \sim L^{3/2}$ . Therefore, following Ref.<sup>46</sup>, we propose the scaling

$$\tilde{\chi}_4^* \sim L^{3/2} f\left(\dot{\gamma}^{-\beta} L^{-3/2}\right), \quad (13)$$

where  $f(x) \sim x$  when  $x \rightarrow 0$  and  $f(x) \sim 1$  when  $x \rightarrow \infty$ . Figure 7 shows that a nice collapse can then be achieved.

Using the fractal dimension  $3/2$  for the cooperative region, one can assess the four-point correlation length,  $\xi_4 \sim \tilde{\chi}_4^{2/3} \sim \dot{\gamma}^{2\beta/3}$ . Interestingly, the exponent  $2\beta/3 \approx 0.6$ , for both scalar and tensorial models, is close to the exponent  $1/2$  extracted by Lemaître and Caroli<sup>33</sup> from the transverse diffusion coefficient in their 2D molecular dynamics simulations (although, admittedly, they found linear avalanches in 2D, instead of our  $3/2$  fractal exponent). On the other hand, it differs from the exponent  $1/4$  predicted by the kinetic elastoplastic theory of Bocquet et al.<sup>5</sup>. More surprisingly, it also differs from the exponent reported in Ref.<sup>46</sup> for a slightly different rescaling of the observable, but with a model identical to the present one. We have checked that the scaling proposed in Ref.<sup>46</sup> provides a poorer fit to our more extensive data set (see Fig. 8).

The insertion of convection modifies the scaling thoroughly. Consistently with the atomistic simulations of Maloney and Lemaître<sup>47</sup>, and Lemaître and Caroli<sup>4</sup>, linear correlations (referred to as “slip lines” by Maloney and Lemaître, see Fig.5)

then dominate and  $\tilde{\chi}_4^*$  saturates at a value apparently almost linear in  $L$  (see Fig.9). The non-saturated regime in which the cooperative volume depends solely on the shear rate, is never truly reached in our simulations : finite-size effects are always dominant, which hampers our search for a scaling law.

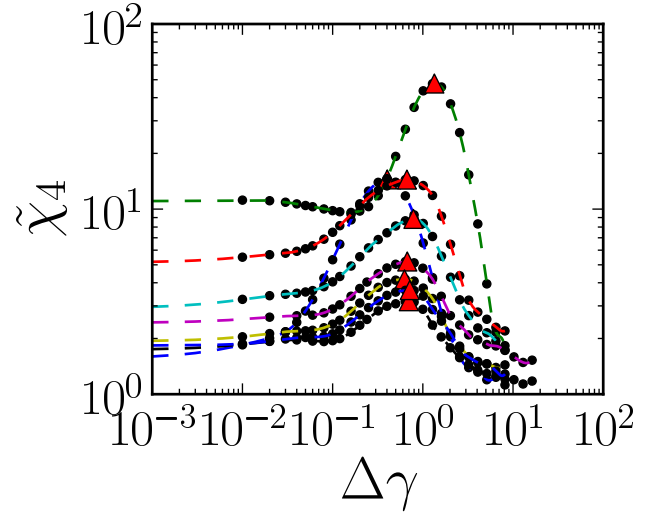
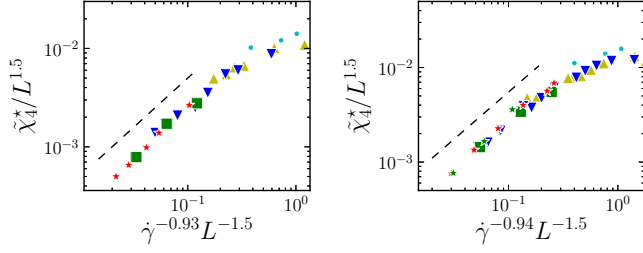


**Figure 6** Four-point susceptibility as a function of strain delay  $\Delta\gamma = \dot{\gamma}\Delta t$ , for various shear rates (increasing  $\dot{\gamma}$  from top to bottom). The red triangles indicate the maximal values.

## 4.2 Cooperative disk

In this section, we propose an alternative protocol to define a correlation length of the system, rooted in the interpretation of the onset of flow in an amorphous solid as a dynamic phase transition<sup>5</sup>. Setting the macroscopic shear stress  $\sigma_{xy}$  as a control parameter, we view the steady-state strain-rate tensor  $\dot{\epsilon}$  as an order parameter, which goes to zero below the yield stress and continuously increases above it.

One may then wonder whether a mean-field approach is applicable, or whether it breaks down because of (spatiotemporal) fluctuations. To answer this question, we assess how large the standard deviation of the fluctuations  $\sqrt{\langle \|\delta\dot{\epsilon}\|^2 \rangle}$  experienced at one point  $M$  in the system is, compared to the mean value  $\|\langle \dot{\epsilon} \rangle\|$  of the order parameter. Except at very large shear rates, this ratio is always large, because plastic events occurring close to  $M$  cause very large fluctuations. But should we only consider the effect of *distant* plastic events, would the fluctuations then be negligible, and a mean-field treatment applicable for them? Concretely, at arbitrary points, we compute the mechanical noise  $\dot{\epsilon}(\xi)$  due to plastic events taking place farther than some distance  $\xi$  from  $M$ . The use of a Ginzburg-Landau criterion  $\sqrt{\langle \|\delta\dot{\epsilon}\|^2 \rangle} / \|\langle \dot{\epsilon} \rangle\|(\xi) < 1$  allows us to distinguish, for any point  $M$  in the system, a cooperative disk of



(a) Static scalar model

(b) Static tensorial model

**Figure 7** Scaling of the maximal cooperative volume  $\tilde{\chi}_4^*$  as a function of shear rate  $\dot{\gamma}$  in the static models. The vertical axis is  $L^{-1.5}\tilde{\chi}_4^*$ , and the horizontal axis is the rescaled shear rate  $\dot{\gamma}^{-\beta}L^{-1.5}$ , with  $\beta = 0.93$  for the scalar model and  $\beta = 0.94$  for the tensorial model. Various linear sizes of the (square) system are studied:  $L =$  (cyan dots) 32, (yellow dots) 64, (blue triangles) 128., (green squares) 192, (red stars) 256, (green stars) 384. As a guide to the eye, we have plotted a dashed line with slope 1.

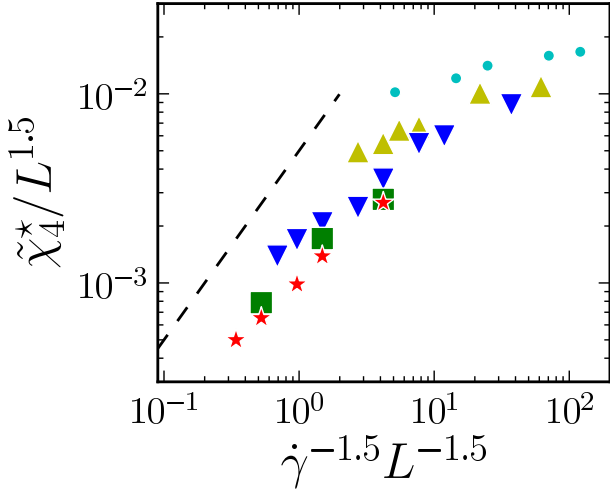


**Figure 8** Test of the scaling of  $\tilde{\chi}_4$  proposed in<sup>46</sup>, viz.,  $\frac{\tilde{\chi}_4}{L^{3/2}} = f\left(\frac{\dot{\gamma}^{-3/2}}{L^{3/2}}\right)$ , for the static scalar model. Various linear sizes of the (square) system are studied:  $L =$  (cyan dots) 32, (yellow dots) 64, (blue triangles) 128., (green squares) 192, (red stars) 256. As a guide to the eye, we have plotted a dashed line with slope 1. Data have been averaged over  $\Delta\gamma \approx 300$ .

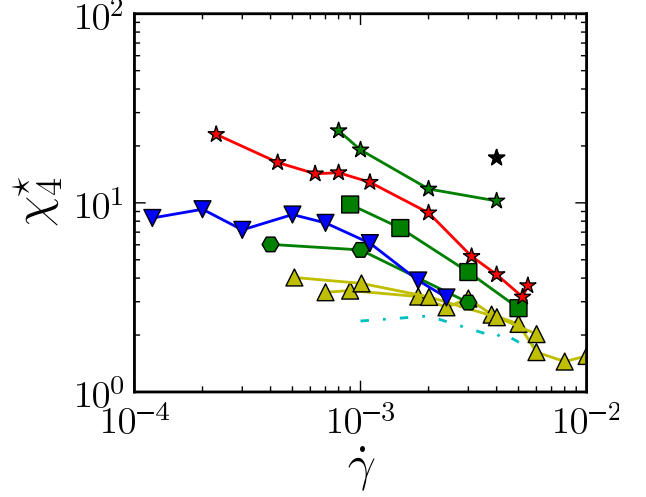


**Figure 9** Maximal cooperative volume  $\tilde{\chi}_4^*$  in the convected tensorial model. Various linear sizes of the (square) system are studied:  $L =$  (cyan dash-dotted line) 32, (yellow triangles) 64, (green hexagons) 96, (blue triangles) 128, (green squares) 192, (red stars) 256, (green stars) 384, (black star) 512.

radius  $\xi^*$ , from an outer region which is amenable to a mean-field treatment, i.e., which satisfies the criterion. With regard to the *instantaneous* mechanical noise at  $M$ , the details of the individual plastic events occurring within the cooperative disk will matter, whereas outside the disk they will not.

In addition, the comparison between the cooperative length  $\xi^*$  and the size of a structural rearrangement (the unit size, here) will be a valuable hint as to whether our model gives credence to mean-field analyses<sup>48</sup>, possibly complemented with a diffusion term to account for spatial fluctuations<sup>5,19,20</sup>.

Figure 10 shows that the data collapse onto a master curve,

$$\frac{\sqrt{\langle \|\delta \dot{\epsilon}\|^2 \rangle}}{\|\langle \dot{\epsilon} \rangle\|}(\xi) \sim \frac{1}{\xi \sqrt{\dot{\gamma}}}. \quad (14)$$

We have checked that this scaling is not marred by finite-size effects. It immediately follows from Eq. 14 that  $\xi^* \sim \dot{\gamma}^{-1/2}$ , which is confirmed by Fig. 11 for all versions of the model. The assumption that plastic events should be only weakly interacting in a slow flow, at low temperature (as expressed in ref<sup>16</sup> and more generally in mean-field-like approaches) may therefore seriously be called into question. An analysis of the impact of these instantaneous fluctuations on the yielding rates is presented in Ref.<sup>49</sup>.

Although the large values of  $\xi^*$  point to the sensitivity to plastic event details over a large region, a simple calculation discarding static spatial correlations between plastic events already provides a satisfactory explanation of the scaling behaviour of  $\xi^*$ , Eq. 14. Indeed, under the assumption of ran-



domly located plastic events, we recover the desired scaling law, Eq. 14, as detailed in Appendix C. The derivation is based on the following: the typical mechanical noise  $\|\dot{\epsilon}\|$  created by a plastic event at a distance  $r$  amounts to  $\frac{\dot{\epsilon}^{pl}}{r^d}$  in  $d$  dimensions, whereas its mean value, for all possible relative positions, is only of order  $\frac{\dot{\epsilon}^{(pl)}}{L^d}$ , because of the compensation between the positive and negative lobes of the elastic propagator; lastly, the average number of simultaneous plastic events is proportional to the shear rate. We would like to emphasise that the scope of the derivation extends far beyond the present model; *in fine*, we simply find that the cooperative length scales with the spacing between homogeneously-distributed, simultaneous plastic events. In other words,  $\xi^*$  is not sensitive to the presence of correlated “slip lines” in the flow and, more generally, other deviations from a homogeneous distribution of plastic events.

It is therefore not a surprise to find the same scaling of the correlation length as that used by Ref.<sup>4</sup> to interpret the transverse diffusivity in their molecular dynamics simulations, namely a dependence on  $\dot{\gamma}^{-1/d}$ . Note that the authors of Ref.<sup>4</sup> had rationalised it by secluding the non-overlapping near-field “flips” (plastic events) from an incoherent background of “flips”. In many respects, our cooperative disk approach comes in the wake of theirs.

### 4.3 Picard’s crossover method

We would like to add a word about the characteristic length introduced by Picard *et al.* in Ref.<sup>24</sup>, namely the linear size of the system below which the macroscopic stress-drops, normalised by the average stress, saturate due to finite-size effects. It seems to us that this saturation occurs when the applied shear rate is decreased to such an extent that there is at most one plastic event in the simulation cell at any time, in which case the characteristic length also provides a measure of the distance between plastic events, in a somewhat cruder way than the cooperative length  $\xi^*$  introduced previously. Accordingly, Picard’s correlation length, assessed in the static scalar model, was also reported to scale with  $\dot{\gamma}^{-1/2}$ .

As a partial summary of the results collected with this first model, we have considered different correlation lengths; all were found to be approximately proportional to the inverse square root of the shear rate, with the exception of the four-point correlation length in the convected system, whose scaling remains elusive for us. How universal is the  $\dot{\gamma}^{-1/2}$ -scaling (in 2D)? Spurred on by this question, we propose a refined model, featuring somewhat more realistic dynamical rules.

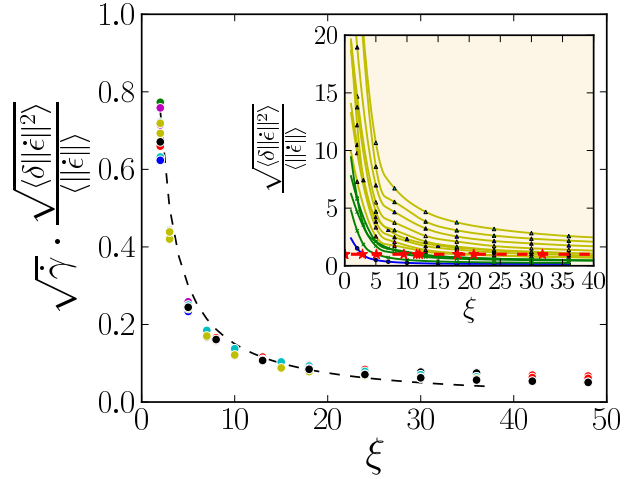


**Figure 10** Ratio of fluctuations over mean value of the mechanical noise due to plastic events taking place farther than  $\xi$ , in the convected tensorial model. System size:  $L = 256$ . Data include points at  $\dot{\gamma} = 5.4 \cdot 10^{-4}, 8.1 \cdot 10^{-4}, 1.2 \cdot 10^{-3}, 1.8 \cdot 10^{-3}, 2.7 \cdot 10^{-3}, 3.5 \cdot 10^{-3}, 4.0 \cdot 10^{-3}, 6.0 \cdot 10^{-3}, 9.0 \cdot 10^{-3}, 1.3 \cdot 10^{-2}, 1.4 \cdot 10^{-2}, 2.0 \cdot 10^{-2}, 1.3 \cdot 10^{-2}, 2.0 \cdot 10^{-2}, 5.6 \cdot 10^{-2}, 2.0 \cdot 10^{-2}, 0.23$ . The dashed black line represents  $y = 1.5/\xi$ . *Inset*: Same data, not rescaled with  $\sqrt{\dot{\gamma}}$ . The yellow ( $\dot{\gamma} < 10^{-2}$ ), green ( $10^{-1} < \dot{\gamma} < 10^{-2}$ ), and blue ( $\dot{\gamma} > 10^{-1}$ ) lines are guides to the eye. The dashed red line marks the limit  $\frac{\sqrt{\langle \|\delta \epsilon\|^2 \rangle}}{\langle \|\epsilon\| \rangle} = 1$ .

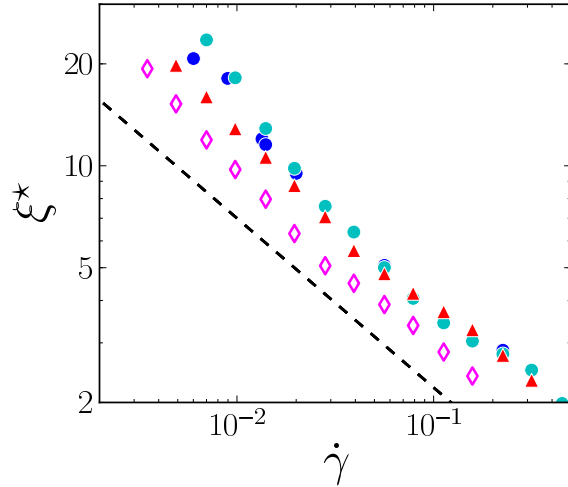


**Figure 11** Dependence of the cooperative length  $\xi^*$  on the applied shear rate  $\dot{\gamma}_{app}$ . The dashed line has slope  $-1/2$ . (Open diamonds) static scalar model; (triangles) static tensorial model; (dots) convected tensorial model. Linear system size:  $L = 128$ , except for dark blue dots ( $L = 256$ ).

## 5 Refinement of the model

The model studied in the previous section does not allow us to recover the Herschel-Bulkley flow curve,  $\sigma = \sigma_0 + A\dot{\gamma}^n$ , with  $n \approx 0.5$ , very often reported in experiments as well as in atomistic simulations, even for athermal materials. Here, we devise a model dedicated mostly to the latter type of materials, insofar as thermal activation of plastic events will be precluded; nevertheless, an extension to thermal fluctuations and ageing in glasses shall also be touched upon.

### 5.1 Onset of a plastic event

The delay  $\tau_{liq}$  before an elastoplastic block yields after crossing the yield stress, as introduced above, is questionable from a potential energy landscape (PEL) perspective. (We must however mention that, to some extent, it has been rationalised in the context of spring-and-dashpot models on a periodic pinning potential, see for instance<sup>50</sup>). Consequently, we replace this criterion with a traditional yield criterion<sup>§</sup>, whereby a block yields as soon as the yield stress is exceeded.

Instead of a single yield stress, a distribution of yield stresses is introduced, on the following basis: let us consider the potential energy landscape and coarse-grain it (for practical reasons) so that too shallow energy basins, of depth  $E_y < E_{min}$ , are discarded. For  $E_y \geq E_{min}$ , following the Soft Glassy Rheology model, we choose an exponential distribution of energy barriers, so that,

$$\rho(E_y) \propto \begin{cases} \exp\left(\frac{E_{min}-E_y}{\langle E_y \rangle}\right) & \text{if } E_y \geq E_{min} \\ 0 & \text{otherwise,} \end{cases} \quad (15)$$

where the mean value  $\langle E_y \rangle$  is adjusted so that mean yield strain takes the realistic value  $\langle \gamma_y \rangle = 0.1$ , for a two-dimensional material. At the end of every plastic event, a new energy  $E_y$  is randomly assigned to the block from the  $\rho$  distribution. Regarding the duration of a plastic event, we make the coarse approximation that, while being sheared, there is a typical distance (measured in terms of local strain) between two successively visited metabasins. Of course, this distance is related to the fineness of the coarse graining, i.e.,  $E_{min}$ . Consequently, we suggest that a plastic event ends when a total strain  $\gamma_c \equiv 2\sqrt{E_{min}}$  (in our units<sup>¶</sup>) has been cumulated in the plastic region, i.e., when  $\int \|2\dot{\epsilon}(t)\| dt = \gamma_c$ . Interestingly, this criterion, albeit rather arbitrary, captures the observed decrease of the rearrangement (T1 event) time at high enough strain rates in bubble clusters<sup>51</sup>.

<sup>§</sup> Note that the distinction between Tresca and von Mises yield criteria breaks down in 2D, both criteria being equivalent for  $d \leq 2$ .

<sup>¶</sup> Both the shear transformation volume and the shear modulus are set to unity, so that  $E_y = \gamma_y^2/4$ .

Figure 12 presents the flow curve resulting from these new dynamical rules, with  $\gamma_c = 0.7 \langle \gamma_y \rangle$ . The curve is perfectly fit by a Herschel-Bulkley equation with exponent  $n \simeq 0.57$  over a reasonable shear rate window. (At higher shear rates, plastic events invade the whole simulation cell, and the dissipative processes during plasticity dominate).

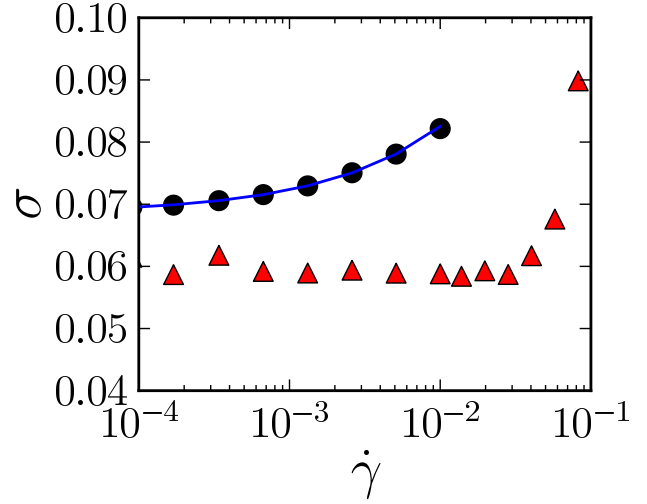


**Figure 12** Flow curves  $\sigma(\dot{\gamma})$  for the convected tensorial model with refined probabilities and no thermal activation ( $x_{loc} = 0$ ). The model parameters are:  $\gamma_c = 0.7$  and (triangles)  $k = 10^{-3}$  or (dots)  $k = \infty$ . The flow curve for the infinite rate of recovery,  $k = \infty$  is fit with a Herschel-Bulkley equation,  $\sigma = 0.07 + 0.19\dot{\gamma}^{0.57}$ .

### 5.2 Thermal activation of plastic events and ageing

Thermally activated plastic events can easily be incorporated into the model. This is achieved by modifying the yielding rate as follows,

$$l(\sigma, t) = \exp\left(\frac{E(\sigma) - E_y}{k_B T}\right), \quad (16)$$

where  $\sigma$  is the local magnitude of the shear stress,  $E(\sigma) \equiv \sigma^2/4$ , and  $k_B T$  is the thermal energy.

In that case, thermally activated rejuvenation of the elastoplastic blocks competes with the possibility to land in a deeper energy basin, and Bouchaud's trap model<sup>52</sup> establishes the existence of a liquid-glass transition at a critical temperature. Below this temperature, the system spends most of the time exploring always deeper wells on average after successive rearrangements, and the prevalence of rearrangement-induced ageing of the material results in a macroscopic yield stress as the shear rate goes to zero.

### 5.3 Ageing and shear-banding

The previous type of ageing requires particles to break out of the cages created by their neighbours (only to end up in an even more rigid cage). In a PEL perspective, this would correspond to successive jumps between metabasins. Yet, one may think that, in some situations, the energy minimisation within one metabasin, via jumps between basins, can be only partially completed as the plastic event terminates, so that short-term ageing can take place in the elastic regime. Physically, candidates for short-term ageing would hypothetically be the re-orientation of particles in a Laponite suspension to maximise the electrostatic or van der Waals interactions or the ion exchanges with the solvents. For foams, it might be the time of recovery of the optimal angles between bubble walls at the Plateau borders, or the equilibration time of the surface tension of the liquid films upon a sudden variation of their area, in the case of foams with high surface modulus surfactants<sup>53</sup>. In granular matter, moisture-induced ageing has been reported in the material at rest<sup>54</sup>. In our approach, short-term ageing shall straightforwardly be modelled by imposing a finite time for the energy barrier  $E_y(t)$  to reach its final value, after a plastic event, as follows,

$$\dot{E}_y(t) = k \frac{E_y - E_y(t)}{E_y - E_{min}}, \quad (17)$$

where  $k$  is a rate of recovery, and stability is supposed to be minimal at the end of a plastic event, that is,  $E_y(t_{end}) = E_{min}$ . Note that the shear-induced lowering of the energy barriers has received at least numerical confirmation<sup>55</sup>.

Qualitatively, the rate of recovery  $k$  is analogous to the inverse of the restructuring time  $\tau_{res}$  introduced in the simple model of section 3. When  $k$  is too low, and the driving  $\dot{\gamma}$  competes with the recovery process, the material will be prone to shear localisation: fracture in a region makes it durably weaker. In Fig. 13, the extent of shear localisation is quantified with the help of the shear-banding observable  $\kappa$  (see Section 3.3). The associated stress plateau on the flow curve is conspicuous in Fig. 12. At extremely low shear rates,  $\dot{\gamma} \ll k$ , one expects to recover a homogeneous flow in the steady state, similar to that for  $k = \infty$ <sup>56</sup>. It is worth noting that Vandembroucq and co-workers<sup>25</sup> too have studied a coarse-grained model with permanent strain weakening, which boils down to  $k = 0$  with our notations, and have also reported that it was associated with shear localisation.

More generally, there is now growing evidence that the longer the material needs to heal back to its pristine state after a plastic event, the more prone it is to shear localisation. The general concept of healing time can take diverse forms in practice: it can be the duration of the rearrangement itself as in Ref.<sup>41,43</sup>, the chemical relaxation time of the local mechanical (e.g., surface tension) properties towards their equilibrium

values after a plastic event (which the authors of Ref.<sup>53</sup> argue results in a flatter flow curve for foams with high surface modulus surfactants, as compared to their low surface modulus counterparts), the thermally activated rebinding of failed contacts<sup>57</sup>, or the time to dissipate the induced heat<sup>58</sup>. Alternatively, in its initial state, the material may have been stabilised by ageing or a careful preparation protocol involving a slow cooling rate, the benefits of which are lost locally upon the occurrence of a plastic event<sup>58</sup>. In this vein, Kumar et al.<sup>59</sup> recently reported that the lower the fictive temperature of a metallic glass, the more brittle it is. Also, attractive interactions are often reported to enhance the heterogeneity of the flow, which may be connected to long time scales to form stable aggregates<sup>60</sup>. But the effect of the increase transcends the variety of these mechanisms.

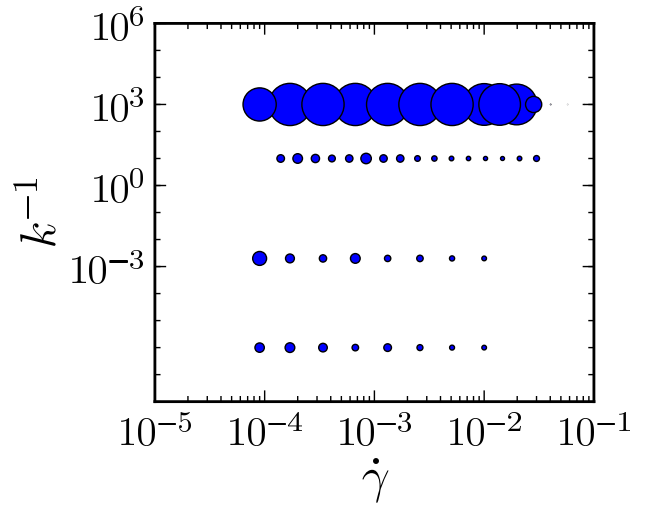


**Figure 13** Dependence of the shear-banding parameter  $\kappa$  on the applied shear rate  $\dot{\gamma}$  and the recovery time  $k^{-1}$ . The largest circle corresponds to  $\kappa = 1$ . The system consists of  $128 \times 128$  blocks.

### 5.4 4-point susceptibility $\chi_4$

Let us now set  $k = \infty$  and investigate the four-point correlations of the stress fluctuations, as in the previous model. The spatial profiles of  $\mathcal{G}_4(r, \Delta t^*)$  (*not shown*) retain the symmetry described above, although in the convected version the cross-wise lobe is now less skewed, owing to the lower yield strain. However, the integrals of  $\mathcal{G}_4(r, \Delta t^*)$  over growing disks centered at the origin scale differently with the disk radii  $R$ ; here they scale with  $R^\alpha$  for  $1 \ll R \ll L$ , with  $\alpha \approx 0.6$  roughly in the static case.

To carry on with the quantitative study, we turn to the maximal cooperative volume  $\tilde{\chi}_4^*$ . Since no obvious scaling was found in the convected case with the previous model, only the

static tensorial model is studied here. For a given system size, say,  $L = 128$ , at relatively high shear rates, the exponent  $\beta$  in  $\tilde{\chi}_4^* \sim \dot{\gamma}^{-\beta}$  is of order 0.2-0.3, that is, significantly lower than its counterpart for the simplistic model. In spite of the scatter of the data, we clearly see that the scaling law used above is no longer valid for this model, as illustrated in Fig. 14; universality in the variations of the cooperative volume with the system size and the shear rate is thus ruled out. In fact, the scaling form  $\frac{\tilde{\chi}_4^*}{L^\alpha} = f\left(\frac{\dot{\gamma}^{-\beta}}{L^\alpha}\right)$  in general does not seem to provide any nice collapse of the data here.

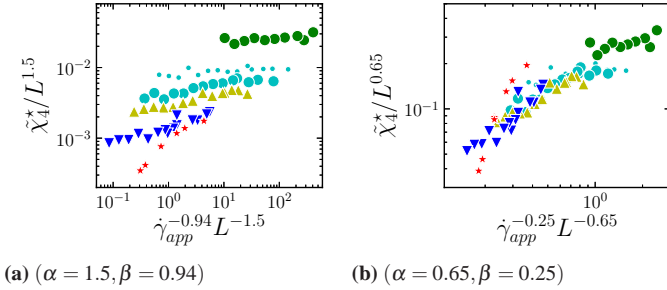


**Figure 14** Maximal cooperative volume  $\tilde{\chi}_4^*$ , rescaled according to  $\frac{\tilde{\chi}_4^*}{L^\alpha} = f\left(\frac{\dot{\gamma}^{-\beta}}{L^\alpha}\right)$ , for two distinct pairs  $(\alpha, \beta)$ : the exponents measured in the previous section,  $(\alpha = 1.5, \beta = 0.94)$ , and better suited exponents,  $(\alpha = 0.65, \beta = 0.25)$ . Various linear sizes of the (square) system are studied:  $L =$  (large green dots) 16, (cyan dots) 32, (large cyan dots) 48, (yellow triangles) 64, (blue triangles) 128, (red stars) 256. As a guide to the eye, we have plotted a dashed line with slope 1. Data have been averaged over  $\Delta\gamma \approx 400\langle\gamma\rangle$ .

## 5.5 Cooperative disk

As for the previous model, we determine, at an arbitrary point  $M$  in the system, the radius  $\xi^*$  of the cooperative disk outside which plastic events contribute to the instantaneous mechanical noise perceived at  $M$  essentially in a mean-field manner.

The inset of Figure 15 shows that the scaling  $\frac{\sqrt{\langle\|\delta\hat{\epsilon}\|^2\rangle}}{\|\langle\hat{\epsilon}\rangle\|}(\xi) \sim \frac{1}{\xi\sqrt{\dot{\gamma}}}$  is also entirely satisfactory in this case. It follows that the scaling of the cooperative length  $\xi^*$  with  $\dot{\gamma}^{-1/2}$  is conserved, although a departure from this scaling is observed when  $\xi^* \gtrsim 20$ , due to finite-size effects (see Fig. 15). This supports the idea that the arguments developed above to ground the scaling of this cooperative length with the spacing between simultaneous plastic events are not model-specific; we expect them to be relevant, for  $\xi^*$ , even in the thermal regime.

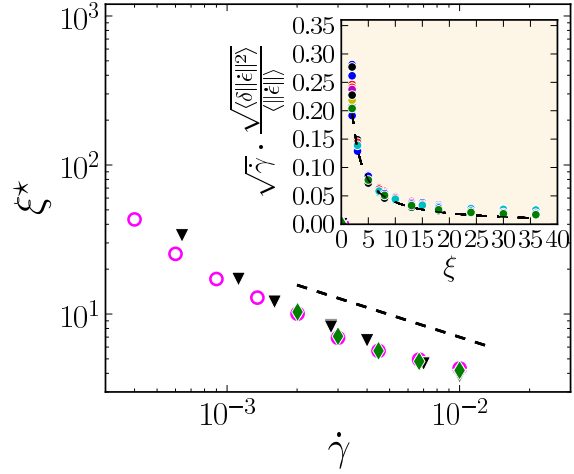


**Figure 15** Cooperative length  $\xi^*$  as a function of the applied shear rate  $\dot{\gamma}$ . Model parameters:  $\gamma_c = 0.07, k = \infty$ , with linear system size  $L =$  (black triangles) 128, (pink circles) 256, (green diamonds) 384. The dashed line has slope -0.5. (Inset) Rescaled fluctuation over mean value ratio  $\sqrt{\dot{\gamma}} \frac{\sqrt{\langle\|\delta\hat{\epsilon}\|^2\rangle}}{\|\langle\hat{\epsilon}\rangle\|}$  as a function of  $\xi$ , for various  $\dot{\gamma}$ . The dashed line represents  $0.39/\xi$ .

## 5.6 Persistent limits of the model, importance of fluctuations, outlook

The refined model presented in this section features an additional source of disorder as compared to the model with simplistic rules presented in Section 3 and studied in Section 4: a distribution of yield stresses. Nevertheless, cooperative effects persist, and fluctuations of the mechanical noise remain large, which may explain why deviations from mean-field behaviours have been reported in the flow of amorphous solids<sup>61,62</sup>.

It must however be said that some other aspects of disorder in these systems are still ignored in our model; accordingly, the spatial correlations that we predict with its help may well be overestimated. Among these other aspects of disorder, let us mention the spatial heterogeneities in shear modulus and the particulate nature of the material at the scale of a shear transformation zone, both of which are expected to alter the elastic propagator that we use. Shear waves are also expected to be damped by the finite viscosity of the (visco)elastic medium, but also by plastic regions, whose softening has been discarded so far in the computation of the elastic propagator. Finally, we have assumed an instantaneous propagation of shear waves.



---

## 6 Conclusion

In this contribution, we have presented a detailed study of diverse variants of a coarse-grained model for the flow of amorphous solids. These models consist of elastic blocks that yield when the local stress gets too large; interaction between the blocks result from the stress redistribution that takes place during the plastic events. In a first version of the model, we have assessed the importance to use a tensorial stress, instead of settling with its component along the macroscopic shear, and to account for the convection of the blocks (in a coarse-grained fashion). In the absence of convection, scalar and tensorial models are extremely similar in terms of flow curve, tendency to shear localisation, and magnitude of spatial correlations. The convected model mainly differs from the static ones because of the restored asymmetry between the flow and velocity-gradient directions: for instance, shear bands can only be aligned along the flow direction, in agreement with experimental observations. The convected model also features enhanced fluctuations, and does not follow the same scaling for the four-point stress susceptibility. In that regard, the influence of the practical way in which convection is implemented in the model may however be determinant.

We have also proposed new dynamical rules to make the model more directly related to real systems. Flow curves more similar to those typically observed in experiments have been obtained; in addition, we have been able to propose a somewhat more general interpretation of the tendency to shear localise as the healing time following a rearrangement increases.

Turning to the correlation lengths, the origin of the decreasing cooperativity as the shear rate increases is that plastic events screen each other. To study the decrease quantitatively, we have defined a cooperative length delimiting a region where the fluctuations due to individual plastic events matter from an outer region which mainly acts in a mean-field way. Along with other prescriptions, this definition gives a correlation length that scales with the spacing between simultaneous plastic events (as assessed to leading order, i.e., for homogeneously distributed plastic events), that is,  $\dot{\gamma}^{-1/2}$  in 2D in the athermal regime; this scaling is robust to model variations. On the other hand, the variations with the system size and the shear rate of the cooperative volume assessed via the four-point stress susceptibility seem to depend largely upon the model that is considered.

One is thus led to the conclusion that, notwithstanding the existence of a major class of correlation lengths that scale with  $\dot{\gamma}^{-1/d}$  in  $d$  dimensions, there exists no universal scaling behaviour which would hold for all correlation length definitions and all systems. The universality observed in the correlations of the mechanical noise field, and expressed by the radius of the cooperative disk  $\xi^*$ , does not extend to more sophisticated observables that would for example quantify the shape and

size of collective plastic events.

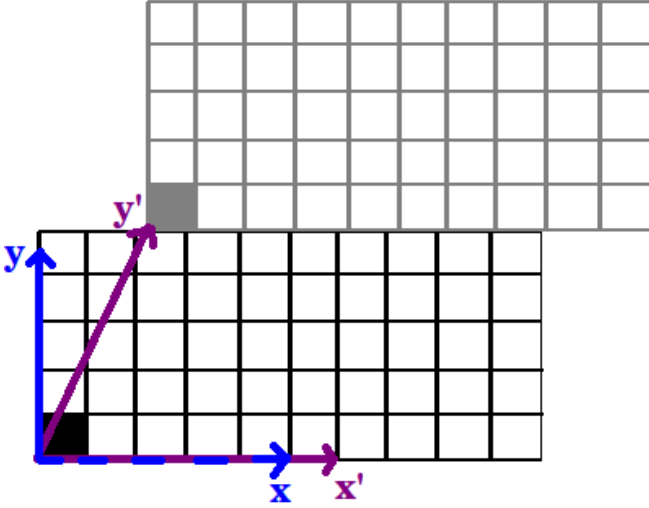
## Acknowledgements

We thank Luca Marradi for help with the computer cluster. J.-L.B. is supported by Institut Universitaire de France and by Grant No. ERC-2011-ADG20110209. Most of the computations presented in this paper were performed using the CIMENT infrastructure (<https://ciment.ujf-grenoble.fr>), which is supported by the Rhône-Alpes region (GRANT CPER07\_13 CIRA: <http://ci-ra.org>).

## References

- [1] L. Berthier, D. Chandler and J. P. Garrahan, *Europhysics Letters (EPL)*, 2005, **69**, 320–326.
- [2] C. Heussinger and J.-L. Barrat, *Physical Review Letters*, 2009, **102**, 218303.
- [3] K. Chen, P. Bak and S. Obukhov, *Physical Review A*, 1991, **43**, 625–630.
- [4] A. Lemaître and C. Caroli, *Physical Review Letters*, 2009, **103**, 065501–065501.
- [5] L. Bocquet, A. Colin and A. Ajdari, *Physical Review Letters*, 2009, **103**, 036001.
- [6] C. Heussinger, P. Chaudhuri and J.-L. Barrat, *Soft matter*, 2010, **6**, 3050–3058.
- [7] H. G. E. Hentschel, S. Karmakar, E. Lerner and I. Procaccia, *Physical Review Letters*, 2010, **104**, 025501.
- [8] A. Argon and H. Kuo, *Materials Science and Engineering*, 1979, **39**, 101–109.
- [9] H. Princen, *Journal of Colloid and Interface Science*, 1985, **105**, 150–171.
- [10] P. Schall, D. A. Weitz and F. Spaepen, *Science (New York, N.Y.)*, 2007, **318**, 1895–9.
- [11] A. Amon, A. Bruand, J. Crassous, E. Clément *et al.*, *Physical review letters*, 2012, **108**, 135502.
- [12] C. E. Maloney and A. Lemaître, *Physical Review E*, 2006, **74**, 016118.
- [13] A. Tanguy, F. Leonforte and J.-L. Barrat, *The European Physical Journal E*, 2006, **20**, 355–364.
- [14] J.-C. Baret, D. Vandembroucq and S. Roux, *Physical Review Letters*, 2002, **89**, 195506.
- [15] M. Falk and J. Langer, *Physical Review E*, 1998, **57**, 7192–7205.
- [16] J. Langer, *Physical Review E*, 2008, **77**, 021502.
- [17] P. Sollich, F. Lequeux, P. Hébraud and M. Cates, *Physical Review Letters*, 1997, **78**, 2020–2023.
- [18] P. Hébraud and F. Lequeux, *Physical Review Letters*, 1998, **81**, 2934–2937.

- 
- [19] S. M. Fielding, M. E. Cates and P. Sollich, *Soft Matter*, 2009, **5**, 2378.
- [20] K. Kamrin and G. Koval, *Physical Review Letters*, 2012, **108**, 178301.
- [21] J. Goyon, A. Colin, G. Ovarlez, A. Ajdari and L. Bocquet, *Nature*, 2008, **454**, 84–7.
- [22] B. Geraud, L. Bocquet and C. Barentin, *The European Physical Journal E*, 2013, **36**, 9845.
- [23] P. Jop, V. Mansard, P. Chaudhuri, L. Bocquet and A. Colin, *Physical Review Letters*, 2012, **108**, 148301.
- [24] G. Picard, A. Ajdari, F. Lequeux and L. Bocquet, *Physical Review E*, 2005, **71**, 010501.
- [25] D. Vandembroucq and S. Roux, *Physical Review B*, 2011, **84**, 134210.
- [26] V. V. Bulatov and A. S. Argon, *Modelling and Simulation in Materials Science and Engineering*, 1994, **2**, 167–184.
- [27] V. V. Bulatov and A. S. Argon, *Modelling and Simulation in Materials Science and Engineering*, 1994, **2**, 185–202.
- [28] V. V. Bulatov and A. S. Argon, *Modelling and Simulation in Materials Science and Engineering*, 1994, **2**, 203–222.
- [29] E. R. Homer and C. A. Schuh, *Acta Materialia*, 2009, **57**, 2823–2833.
- [30] E. R. Homer, D. Rodney and C. A. Schuh, *Physical Review B*, 2010, **81**, 064204.
- [31] L. Berthier, *Physcs Online Journal*, 2011, **4**, 42.
- [32] H. Princen, *Journal of Colloid and interface science*, 1983, **91**, 160–175.
- [33] A. Lemaître and C. Caroli, *Physical Review E*, 2007, **76**, 036104.
- [34] M. Tsamados, A. Tanguy, F. Léonforte and J.-L. Barrat, *The European physical journal. E, Soft matter*, 2008, **26**, 283–93.
- [35] A. Nicolas and J.-L. Barrat, *Physical Review Letters*, 2013, **110**, 138304.
- [36] A. Nicolas and J.-L. Barrat, *Faraday Discuss.*, 2013, **167**, 567–600.
- [37] M. Tsamados, *The European Physical Journal E*, 2010, **32**, 165–181.
- [38] G. Picard, A. Ajdari, F. Lequeux and L. Bocquet, *The European physical journal. E, Soft matter*, 2004, **15**, 371–81.
- [39] D. Barthès-Biesel, *Microhydrodynamique et fluides complexes*, Les Editions de l’Ecole Polytechnique, 2010.
- [40] F. Puosi, J. Rottler and J.-L. Barrat, *ArXiv e-print 1402.1474*, 2014.
- [41] K. Martens, L. Bocquet and J.-L. Barrat, *Soft Matter*, 2012, **8**, 4197–4205.
- [42] P. Chaudhuri and J. Horbach, *Physical Review E*, 2013, **88**, 040301.
- [43] P. Coussot and G. Ovarlez, *The European physical journal. E, Soft matter*, 2010, **33**, 183–8.
- [44] C. Toninelli, M. Wyart, L. Berthier, G. Biroli and J.-P. Bouchaud, *Physical Review E*, 2005, **71**, 041505.
- [45] A. Furukawa, K. Kim, S. Saito and H. Tanaka, *Physical Review Letters*, 2009, **102**, 016001.
- [46] K. Martens, L. Bocquet and J.-L. Barrat, *Physical Review Letters*, 2011, **106**, 156001.
- [47] C. Maloney and A. Lemaître, *Physical Review Letters*, 2004, **93**, 016001.
- [48] K. A. Dahmen, Y. Ben-Zion and J. T. Uhl, *Physical Review Letters*, 2009, **102**, 175501.
- [49] A. Nicolas, K. Martens and J.-L. Barrat, *arXiv preprint arXiv:1401.6340*, 2014.
- [50] P. Marmottant and F. Graner, *Soft Matter*, 2013, **9**, 9602–9607.
- [51] A.-L. Biance, S. Cohen-Addad and R. Höhler, *Soft Matter*, 2009, **5**, 4672.
- [52] J.-P. Bouchaud, *Journal de Physique I*, 1992, **2**, 1705–1713.
- [53] N. D. Denkov, S. Tcholakova, K. Golemanov, K. Ananthpadmanabhan and A. Lips, *Soft Matter*, 2009, **5**, 3389–3408.
- [54] L. Bocquet, E. Charlaix, S. Ciliberto and J. Crassous, *Nature*, 1998, **396**, 735–737.
- [55] D. Rodney and T. Schröder, *The European Physical Journal E*, 2011, **34**, 1–7.
- [56] V. Chikkadi, S. Mandal, B. Nienhuis, D. Raabe, F. Varnik and P. Schall, *EPL (Europhysics Letters)*, 2012, **100**, 56001.
- [57] F. Kun, H. Carmona, J. Andrade Jr and H. Herrmann, *Physical review letters*, 2008, **100**, 094301.
- [58] F. Shimizu, S. Ogata and J. Li, *Acta materialia*, 2006, **54**, 4293–4298.
- [59] G. Kumar, P. Neibecker, Y. H. Liu and J. Schroers, *Nature communications*, 2013, **4**, 1536.
- [60] E. Irani, P. Chaudhuri and C. Heussinger, *arXiv preprint arXiv:1312.4819*, 2013.
- [61] J. Lin, A. Saade, E. Lerner, A. Rosso and M. Wyart, *Europhysics Letters (EPL)*, 2014, **105**, 26003–26009.
- [62] Z. Budrikis and S. Zapperi, *Physical Review E*, 2013, **88**, 062403.



## A Derivation of the elastic propagator in the deformed frame

In order to avoid a spurious discontinuity at the edge of the (periodic) simulation cell when convection is included, the cell must be deformed, in a fashion equivalent to Lees-Edwards boundary conditions in atomistic simulations: periodic replicas of the system in the velocity gradient-direction shall be displaced along the flow, while replicas in the flow direction remain unaffected. At a given time, the elastic propagator shall then be expressed in a deformed frame, with (contravariant) coordinates  $(x', y') = (x - \gamma y, y)$ , where  $\gamma$  is the average shear strain experienced by the cell. Here, unprimed quantities refer to the initial orthonormal frame. The corresponding transformation of the (covariant) Fourier wavenumbers reads  $q' \equiv (q'_x, q'_y) = (q_x, q_y + \gamma q_x)$ .

The metric tensor,

$$(g_{ij}) \equiv \frac{\partial s^k}{\partial s'^i} \frac{\partial s^l}{\partial s'^j} \delta_{kl} = \begin{pmatrix} 1 & \gamma \\ \gamma & 1 + \gamma^2 \end{pmatrix}, \quad (18)$$

where  $s = q$  or  $s = (x, y)$ , is a convenient tool to compute distances in the deformed frame; it relates covariant and contravariant quantities,  $x'_j = g_{ij} x^i$  as well as  $q'_j = g_{ij} q^i$ , for  $i, j \in \{x, y\}$ . When  $\gamma \neq 0$ , the metric tensor  $g_{ij}$  differs from identity, so that  $q'_i \neq q^i$ . Nevertheless, provided that this difference is accepted, Eq. 7 still holds, *viz.*

$$u^i(q') = \frac{-2i}{q'^4} \left[ q'^2 q'_k \epsilon'^{(pl)ki}(q') - q'^i q'_k q'_l \epsilon'^{(pl)kl}(q') \right], \quad (19)$$

from which the strain tensor  $\epsilon'^{ij} = \frac{q'^i u'^j + q'^j u'^i}{2}$  and the elastic (deviatoric) stress  $\sigma'^{ij} = 2\mu \left( \epsilon'^{ij} - \epsilon'^{(pl)ij} \right)$  readily follow.

As in Eq. 6, the dots indicating time derivatives have been dropped in Eq. 19. Finally, the *components* of the stress tensor (and not the *coordinates* of the points at which it is evaluated) are to be expressed in the original, orthogonal basis  $(x, y)$ , as follows:

$$\begin{aligned} \sigma^{ij}(q') &= \frac{\partial x^i}{\partial x'^r} \frac{\partial x^j}{\partial x'^s} \sigma'^{rs}(q') \\ &= \frac{2\mu}{q'^4} \left[ q'^2 \left( \mathcal{A}_u \mathcal{P}^j \epsilon^{(pl)ui}(q') + \mathcal{A}_u \mathcal{P}^i \epsilon^{(pl)uj}(q') \right) \right. \\ &\quad \left. - 2 \mathcal{P}^i \mathcal{P}^j \mathcal{A}_u \mathcal{A}_v \epsilon^{(pl)uv}(q') \right] - 2\mu \epsilon^{(pl)ij}(q'). \quad (20) \end{aligned}$$

Note that we have used the shorthands  $q'^2 = q'_k q'^k = q^2$ ,  $\mathcal{P}^i \equiv \frac{\partial x^i}{\partial x'^r} q^r$ , and  $\mathcal{A}_u \equiv \frac{\partial x'^k}{\partial x^u} q_k = (q_x, q_y - \gamma q_x)$ .

Explicit evaluation of Eq. 20 with the metric tensor (18) leads to our final result:

$$\begin{pmatrix} \sigma^{xx} \\ \sigma^{xy} \end{pmatrix} (q') = \mathcal{G}^\infty \cdot \begin{pmatrix} \epsilon^{pl,xx} \\ \epsilon^{pl,xy} \end{pmatrix} (q'), \quad (21)$$

with

$$\mathcal{G}^\infty \equiv \frac{1}{q'^4} \begin{bmatrix} -(q_x'^2 - q_y'^2)^2 & -2q'_x q_y'^{(y)} (q_x'^2 - q_y'^2) \\ -2q'_x q_y'^{(y)} (q_x'^2 - q_y'^2) & -4q_x'^2 q_y'^{(y)2} \end{bmatrix} \quad (22)$$

and  $q_y'^{(y)} \equiv (q'_y - \gamma q'_x)$ .

With biperiodic boundary conditions, this propagator results in periodic images of the plastic events that are not aligned along the velocity gradient direction, but tilted with an “angle”  $\gamma$ . Besides the (long-range) effect of these periodic images, the shape of the elastic propagator in real space should in principle be insensitive to the frame in which it is computed. However, we would like to indicate that the discrete nature and the symmetries of the meshgrid that we use introduce some near-field dependence of  $\mathcal{G}^\infty$  on  $\gamma$ , up to a distance of few meshes away from the origin of the plastic event. It is therefore important to keep  $\gamma$  within a relatively narrow range, here,  $[-1/2, 1/2]$ , which is achieved thanks to the periodicity of the system in the flow direction.

## B Calculation of the displacement of streamlines induced by plastic events

The deformation is not strictly affine in the system. Consequently, on top of the average deformation of the cell, we need to compute the displacement of each streamline so as to be able to shift it adequately with respect to its neighbours. The average (non-affine) displacement in the flow direction  $x$  on

streamline  $y_0$  that is induced by plastic events reads,

$$\begin{aligned}\langle u_x \rangle_x(y_0) &\equiv L^{-1} \int u_x(x, y_0) dx \\ &= \sum_{q_y} u_x(q_x = 0, q_y) e^{iq_y y_0} \\ &= \sum_{q_y} \frac{-2i}{q_y} \varepsilon_{xy}^{(pl)}(q_x = 0, q_y) e^{iq_y y_0},\end{aligned}$$

where the sums run over all relevant wavenumbers  $q_y = 2\pi n/L$  and, as is now usual, we have dropped the (1)-superscripts and the hats denoting Fourier transforms. To obtain the last equality, we have made use of Eq. 7. Finally, one arrives at,

$$\begin{aligned}\langle u_x \rangle_x(y_0) &= \sum_{q_y} \frac{-2i}{q_y} e^{iq_y y_0} \\ &\quad \times \left[ L^{-1} \sum_{y_{ev}} \left\langle \varepsilon_{xy}^{(pl)}(x, y_{ev}) \right\rangle_x e^{-iq_y y_{ev}} \right] \\ &= \frac{-2i}{L} \sum_{y_{ev}} \left\langle \varepsilon_{xy}^{(pl)} \right\rangle_x(y_{ev}) \sum_{q_y} \frac{e^{iq_y(y_0 - y_{ev})}}{q_y} \\ &= \sum_{y_{ev}} \text{sign}(y_0 - y_{ev}) \\ &\quad \times \left( 1 - \frac{2|y_0 - y_{ev}|}{L} \right) \left\langle \varepsilon_{xy}^{(pl)} \right\rangle_x(y_{ev}),\end{aligned}$$

where the sum runs over all streamlines  $y_{ev}$  and, to get the last line, we have summed the second series over all  $q_y = 2\pi n/L$ ,  $n \in \mathbb{Z}^*$ .

Whenever the cumulative displacement of a streamline in the flow direction reaches the size of a block, it is shifted. As a technical detail, note that we also regularly add a random displacement offset to *all* lines in order to prevent the spurious pinning in the simulation cell of the streamlines that have zero average velocity. Otherwise, this spurious pinning might have jeopardised the translational invariance of the system along the velocity gradient direction.

### C Estimation of the cooperative length $\xi^*$

Simple arguments based on the crude assumption of randomly distributed plastic events explain the importance of the mechanical noise fluctuations measured at an arbitrary point, say the origin  $M$ , and the scaling law in  $d = 2$  dimensions, Eq. 14, which is recalled here:

$$\frac{\sqrt{\langle \|\delta \dot{\varepsilon}\|^2 \rangle}}{\|\langle \dot{\varepsilon} \rangle\|}(\xi) \sim \frac{1}{\xi \sqrt{\gamma}}. \quad (23)$$

Denoting by  $p \in [0, 1]$  the average surface fraction covered by plastic events at a given shear rate and calling  $\dot{\varepsilon}^{pl} \sim \frac{\dot{\gamma}}{\tau}$  the

typical plastic strain rate, the mean value of the mechanical noise due to plastic events occurring farther than  $\xi$  is:

$$\begin{aligned}\|\langle \dot{\varepsilon} \rangle\| &\approx \int_{\xi}^L \int_{\mathcal{S}^d} \frac{p \dot{\varepsilon}^{pl}}{L^d} r^{d-1} dr d\theta \\ &\sim \frac{p \dot{\varepsilon}^{pl} (L^d - \xi^d)}{L^d}.\end{aligned}$$

Here,  $\mathcal{S}^d$  denotes the unit sphere in  $d$  dimensions, and we have used that the spatially averaged contribution of a plastic event to the stress field is of order  $\frac{\varepsilon^{pl}}{L^d}$ . Numerical prefactors are omitted.

Let us now turn to the fluctuations and start by computing  $\delta \dot{\varepsilon}(r)$ , the contribution of plastic events taking place in a shell  $[r, r+1]$  centred at  $M$ :

$$\begin{aligned}\delta \dot{\varepsilon}(r)^2 &= \left( \int_r^{r+1} dr' \int_{\mathcal{S}^d} r'^{d-1} d\theta \mathcal{G}(r', \theta) n(r', \theta) \dot{\varepsilon}^{pl} \right)^2 \\ &\sim 0 + \int_r^{r+1} dr' \int_{\mathcal{S}^d} r'^{d-1} d\theta \left( \frac{\cos(4\theta)}{r^d} n(r, \theta) \dot{\varepsilon}^{pl} \right)^2 \\ &\sim \frac{p \cdot (\dot{\varepsilon}^{pl})^2}{r^{d+1}},\end{aligned}$$

where  $n(r', \theta) = 0$  or  $1$  is the plastic activity at point  $(r', \theta)$ , and, crudely, we have assumed the absence of static spatial correlations between plastic events outside a fully correlated unit volume  $r'^{d-1} dr' d\theta = 1$ , i.e., the volume of a single plastic event.

The sum  $\delta \dot{\varepsilon}$  of the contributions of the concentric shells of radius  $r \geq \xi$  then reads:

$$\begin{aligned}\delta \dot{\varepsilon}^2 &\sim \left[ \sum_{r=\xi}^L \delta \dot{\varepsilon}(r) \right]^2 \\ &\sim \sum_{r=\xi}^L \delta \dot{\varepsilon}(r)^2 \\ &\sim p \cdot (\dot{\varepsilon}^{pl})^2 \left[ \frac{L^d - \xi^d}{L^d \xi^d} \right].\end{aligned}$$

We are now able to compute the fluctuations-to-average ratio in the limit  $\xi \ll L$ ,

$$\frac{\sqrt{\delta \dot{\varepsilon}^2}}{\|\langle \dot{\varepsilon} \rangle\|} \sim \frac{1}{\xi^{d/2} \sqrt{p}}. \quad (24)$$

To conclude, one just has to recall that, when thermal fluctuations are negligible, the density of plastic events is proportional to  $\dot{\gamma}$ , because the typical stress release per plastic event  $\varepsilon^{pl}$  shows no significant dependence on the applied shear rate.



